Phospholipid bicelles improve the conformational stability of rhodopsin mutants associated with retinitis pigmentosa

Xiaoyun Dong, Eva Ramon, Maria Guadalupe Herrera-Hernández[†] and Pere Garriga[*]

Grup de Biotecnologia Molecular i Industrial, Centre de Biotecnologia Molecular, Departament d'Enginyeria Química, Universitat Politècnica de Catalunya, Edifici Gaia, Rambla de Sant Nebridi 22, 08222 Terrassa, Catalonia, Spain.

[†]***Permanent address****: Unidad de Biotecnología, Campo Experimental Bajío (INIFAP). Km 6.5 Carretera Celaya-San Miguel Allende s/n México. CP 38110*

[*]***Correspondence to****:* Professor Pere Garriga, Grup de Biotecnologia Molecular i Industrial, Centre de Biotecnologia Molecular, Departament d'Enginyeria Química, Universitat Politècnica de Catalunya, Rambla de Sant Nebridi 22, 08222 Terrassa, Spain. Tel: +34 937398568; FAX: +34 937398225; E-mail: pere.garriga@upc.edu

Keywords: retinal proteins, ligand binding, retinal degeneration, phospholipids, stability.

Funding source: This work was supported by grants from Ministerio de Ciencia e Innovación (Spain) (SAF2011-30216-C02-01), Grups de Recerca Consolidats from Generalitat de Catalunya (2009 SGR 1402), and Fundación Areces (to PG), and by a CIG grant from the EUROPEAN Commission (to ER). XD is the recipient of a predoctoral scholarship from the Chinese Scholarship Council (CSC). MGHH is the recipient of a predoctoral scholarship from CONACYT Mexico.

AB STRACT

Mutations in the visual photoreceptor rhodopsin are the cause of the retinal degenerative disease retinitis pigmentosa. Some naturally-occurring mutations can lead to protein conformational instability. Two such mutations, N55K and G90V, in the first and second transmembrane helices of the receptor, have been associated with sector and classical retinitis pigmentosa respectively, and showed enhanced thermal sensitivity. We have carefully analyzed the effect of phospholipid bicelles on the stability and ligand-binding properties of these two mutants and compared it with those of the detergent-solubilized samples. We have used a phospholipid bilayer constituted of 1,2-dimyristoyl-*sn*-glycero-3-phosphatidylcholine (DMPC) and 1,2-dihexanoyl-*sn*-glycero-3-phosphocholine (DHPC) bicelles system. We find that DMPC/DHPC bicelles dramatically increase the thermal stability of the rhodopsin mutants G90V and N55K. The chromophore stability and regeneration of the mutants were also increased in bicelles when compared to their behavior in dodecyl maltoside detergent solution. The retinal release process was slowed down in bicelles and chromophore entry, after illumination, was improved for the G90V mutant but not for N55K. Furthermore, fluorescence spectroscopy measurements showed that bicelles allowed more exogenous retinal binding to photoactivated G90V mutant than in detergent solution. In contrast, N55K could not re-position any chromophore either in detergent or in bicelles. The results demonstrate that DMPC/DHPC bicelles can counteract the destabilizing effect of the disease-causing mutations and can modulate the structural changes ensuing receptor photoactivation in a distinct specific manner for different retinitis pigmentosa mutant phenotypes.

ABBREVIATIONS

GPCRs, G-protein-coupled receptors; RP, retinitis pigmentosa; sector RP, sector retinitis pigmentosa; ROS, rod outer segment; Rho, rhodopsin; WT, wild type; DMPC, 1,2-dimyristoyl-*sn*-glycero-3-phosphatidylcholine; DHPC, 1,2-dihexanoyl-*sn*-glycero-3-phosphocholine; DM, *n*-dodecyl-D-maltoside; SB, Schiff base; BTP, bis-tris-propane; SDS-PAGE, SDS polyacrylamide gel electrophoresis; MetaII, Metarhodopsin II.

INTRODUCTION

The visual photoreceptor rhodopsin (Rho) is a prototypical member of the G-protein-coupled receptors (GPCRs) superfamily responsible for scotopic (or dim-light) vision. As a model of GPCRs, Rho has been extensively studied, and since the first report of its crystal structure, several GPCRs structures have been solved by X-ray crystallography [1–5]. Rho is found in the rod outer segment (ROS) membranes of the photoreceptor cells of the retina where it is embedded in the lipid bilayer surrounded by ~65-70 phospholipids per protein molecule [6–9]. Rho consists of the opsin apoprotein and the 11-*cis*-retinal ligand which is covalently bound through a protonated Schiff base (SB) linkage to K296 at the seventh transmembrane helix of the photoreceptor [10–12]. Upon photon absorption, the 11-*cis* retinal chromophore isomerizes to all-*trans*-retinal and triggers a conformational change in the receptor that leads to the active metarhodopsin II (MetaII) photointermediate which can bind and activate the G-protein transducin [11,13]. Mutations in Rho are one of the main causes of retinitis pigmentosa (RP), which is a genetically heterogeneous disorder involving rod photoreceptor cell death and eventually leading to blindness [14]. The worldwide prevalence of RP is about one in 4000 [10,15]. Misfolding and misassembly of mutant Rho, associated with RP, alters the cellular fate and induces cell death [16,17]. Some mutations alter the trafficking ability from the endoplasmic reticulum to the plasma membrane [18]. Sector retinitis pigmentosa (sector RP) is an atypical variant of RP. In sector RP, only isolated areas of the fundus show pigmentary changes. It is characterized by regionalized areas of bone spicule pigmentation usually found in the inferior quadrants of the retina, abnormal electro-retinograms, visual-field defects, and slow to no degeneration [19].

Structure-function studies of Rho are typically carried out in the mild dodecyl maltoside (DM) detergent solution [20,21]. However, membrane proteins often show poor

conformational stability, and can lose activity or even denature in detergent micelles [22,23]. Membrane-like environments help maintaining the proper structure and biochemical function of membrane proteins and their mutants [24,25]. Phospholipid bicelles have been shown to improve the stability of Rho [26–28], and for this reason we have studied two Rho mutants, G90V and N55K, and compared their properties in DM detergent and in DMPC/DHPC bicelles (Figure 1). G90V (causing RP phenotype) and N55K (associated with sector RP) show structural instability in the dark and thermal sensitivity [21,29,30]. 9-*cis*-retinal was used as an exogenous analog [31,32] for a detailed characterization of these two specific Rho mutants. The thermal stability and chromophore regeneration ability of G90V and N55K improved in DMPC/DHPC bicelles, which provided a suitable bilayer environment for the mutants. MetaII decay experiments of G90V mutant in bicelles showed additional fluorescence increase upon hydroxylamine addition after complete retinal release but not for the N55K mutant. This suggested conformational differences in the photoactivated receptors affecting retinal accessibility to the post-bleached opsin retinal-binding pocket. Furthermore, the photoactived opsin conformation of the G90V RP mutant would be more efficient in allowing retinal entering into the opsin binding pocket when the protein is in DMPC/DHPC bicelles than when it is in DM detergent solution. In contrast, N55K opsin, in DMPC/DHPC bicelles, did not allow any chromophore entrance in the opsin binding pocket. Overall, the results obtained indicate that DMPC/DHPC bicelles offer a stable bilayer environment for mutants associated with RP but specific conformational differences can be observed for the two mutants, especially after photoactivation, which could be related to their different clinical phenotypes.

EXPERIMENTAL PROCEDURES

Materials

Rho was purified from bovine retinas, which were obtained from J.A. Lawson (Lincoln, NE). WT, G90V and N55K opsin genes were cloned into the pMT4 vector. The chromophore 11-*cis*-retinal was provided by Dr. R. Crouch (National Eye Institute, National Institutes of Health, USA). 9-*cis*-retinal was purchased from Sigma-Aldrich. 1,2-dimyristoyl-*sn*-glycero-3-phosphocholine, DMPC(14:0) and 1,2-dihexanoyl-*sn*-glycero-3-phosphocholine, DHPC(6:0) were purchased from Avanti Polar Lipids Inc (Alabaster, AL, USA) and *n*-dodecyl-D-maltoside (DM) was from Anatrace (Maumee, OH, USA).

Purified mAb rho-1D4 was provided by Cell Essentials (Boston, MA, USA) and was coupled to CNBr-activated Sepharose 4B Fast Flow following the manufacturer's instructions (Amersham Biosciences, USA). Secondary antibody goat anti-mouse IgG-HRP conjugated was purchased from Santa Cruz Biotechnology (Heidelberg, Germany). The 1D4 9-mer peptide corresponding to the last 9 amino acids of Rho (TETSQVAPA) was synthesized by Serveis Cientificotècnics (Universitat de Barcelona, Spain). Hydroxylamine, protease inhibitor cocktail, phenylmethanesulfonyl (PMSF), and bis-tris-propane (BTP) were from Sigma-Aldrich (St. Louis, MO, USA). Polyethyleneimine 25 kDa (PEI) was purchased from Polysciences (Warrington, PA, USA).

Buffers

The following buffers were used: buffer A: 10 mM bis-tris-propane (BTP), 140 mM NaCl, 2mM $MgCl_2$, 2 mM $CaCl_2$, pH 6.0; DM buffer: buffer A containing 0.05% (w/v) DM; bicelles buffer: buffer A containing 2% (w/v) DMPC/DHPC bicelles; solvent buffer: 137 mM NaCl, 2.7 mM KCl, 1.5 mM KH_2PO_4, and 8 mM Na_2HPO_4, pH 7.4.

Cell culture materials

COS-1 cells were obtained from the American Type Culture Collection (Manassas, VA, USA). DMEM, serum and antibiotics were from Sigma-Aldrich (St. Louis, MO, USA), OPTIMEM reduced serum media was from Life Technologies (Madrid, Spain).

Bicelles preparation

A 10% (w/v) DMPC sample was prepared by dissolving the powder in buffer A and gently vortexing, followed by incubating the solution at 42°C for 5 min and then cooling to room temperature. 10% (w/v) DHPC was also prepared in buffer A. Final 2% (w/v) DMPC/DHPC (1:1) mixtures were mixed briefly, heated to 42°C for 10 min, and then left to stir at room temperature for 1 h until the mixtures were clear (bicelles buffer). All bicelles solutions were used within 36 h from preparation [26].

Expression, purification and preparation of Rho, and recombinant WT and mutants

Rho refers to native Rho purified from bovine retinas whereas WT refers to recombinant Rho heterologously expressed in COS-1 cells, immunopurified and regenerated with 9-*cis*- retinal.

Rho purification. ROS membranes were purified from bovine retinas using a sucrose gradient method under dim red light. The membranes were suspended in 70 mM potassium phosphate, 1mM $MgCl_2$, 0.1mM EDTA, pH 6.9, then subsequently centrifuged and the pellets were resuspended in 5 mM Tris-HCl (pH 7.5) containing 0.5 mM $MgCl_2$. Two alternating washes with these buffers were carried out to remove any further contaminating proteins. Finally, ROS membranes were split into several aliquots and stored in the dark at -20°C. The ROS membranes were used for Rho purification. ROS membranes were solubilized in solvent buffer with 1% (w/v) DM in the dark for 1 h at 4°C. Then the sample was centrifuged at 35000 rpm (50 Ti rotor) for 30 min at 4°C in order to get rid of any unsolubilized material. The soluble fraction was incubated

with the 1D4-Sepharose beads for 3 h and the purified protein was eluted in either DM buffer or bicelles buffer containing 100 μM 1D4 9-mer peptide. All the procedures were performed in the dark on ice.

WT, and G90V and N55K mutants purification. WT opsin, and G90V and N55K mutants were constructed on a synthetic bovine opsin gene in the pMT4 vector [33]. The WT, and the G90V and N55K opsin mutants were transiently expressed in COS-1 cells by chemical transfection using PEI reagent as previously described [34,35]. After 48 h, the cells were harvested and regenerated with 10 μM 9-*cis*-retinal in solvent buffer with overnight incubation. Then the intact cells were solubilized in solvent buffer with 1% DM(w/v) containing 100 μM PMSF and protease inhibitors, followed by ultracentrifugation for 30 min in an Optima LE-80K Ultracentrifuge (Beckman Coulter) at 30,000 rpm (50 Ti rotor). The supernatants were used for immunoaffinity chromatography purification with Sepharose coupled to rho-1D4 antibody. The pigments were eluted, three hours after incubation, with 100 μM 1D4 9-mer peptide in DM buffer or in bicelles buffer. All the procedures were performed in the dark on ice. The samples in DM buffer and bicelles buffer were stored on ice and used within 36 h.

UV-visible absorption and fluorescence spectroscopies

UV-vis spectra were obtained with a Cary 100Bio spectrophotometer (Varian, Australia), equipped with water-jacketed cuvette holders connected to a circulating water bath. Temperature was controlled by a Peltier accessory connected to the spectrophotometer. All spectra were recorded in the 250nm-650nm range with a bandwidth of 2nm, a response time of 0.1s, and a scan speed of 300nm/min. The spectral ratio is defined as the absorbance at 280nm divided by the absorbance at the visible λ_{max} value in order to measure the pigment yield and the chromophore stability

after purification. These samples were used for photobleaching, thermal bleaching, chromophore regeneration, MetaII decay and chromophore entry experiments.

All fluorescence assays were performed by using a Photon Technologies QM-1 steady-state fluorescence spectrophotometer (PTI Technologies, Birmingham, NJ, USA). Sample temperature was controlled with a TLC 50 Peltier accessory (Quantum Northwest, Liberty Lake, WA, USA) connected to a hybrid liquid coolant system Reserator XT (Zalman, Garden Grove, CA, USA). Trp fluorescence was monitored over time. All fluorescence scans were carried out by exciting the samples for 2s at 295nm with a slit of 0.5nm, and blocking the excitation beam for 28s with a beam shutter to avoid photobleaching of the sample. Trp emission was monitored at 330 nm with a slit of 10nm.

Western blot of WT and mutants in DM detergent and in bicelles

WT, G90V and N55K mutants were purified as described in either DM buffer or bicelles buffer. Then, 100 ng of purified protein were mixed with loading buffer and loaded onto a SDS-PAGE gel. After electrophoresis, the proteins were transferred to a nitrocellulose membrane and the protein bands visualized with the appropriate antibodies. Rho 1D4 antibody dilution of 1:10,000 was used for opsin detection and the secondary antibody was goat anti-mouse HRP with a 1:5,000 dilution. Both antibodies were dissolved in TBS with 0.1% (v/v) Tween buffer. Blots were developed using super-signal west pico chemiluminescent substrate (Thermo Fisher Scientific, USA).

Thermal bleaching assay of the purified proteins

The thermal stability of Rho, WT and its mutants was followed by means of UV-visible spectrophotometry. Pigment thermal bleaching rates were obtained, in the dark, by monitoring the decrease of absorbance at λ_{max} of the visible spectral band as a function of time at either 55°C or 37°C. Spectra were recorded every min. Data points were

obtained by using the equation: $\Delta A = (A-A_f)/(A_0-A_f)$, where A is the absorbance recorded at λ_{max}, A_f is the absorbance at the final time, and A_0 is the absorbance at time 0. The half-life time ($t_{1/2}$) for the process was determined by fitting the experimental data to single exponential decay curves using Sigma Plot version 11.0 (Systat Software, Chicago, IL, USA).

Regeneration of WT, G90V and N55K

2.5 fold molar excess of 9-*cis*-retinal was added to the purified samples, in the dark, followed by illumination with a 150-watt power source equipped with an optic fiber guide, using a >495 nm cut-off filter to avoid photobleaching of the free retinal. The samples were illuminated for 30s at 20°C and spectra were recorded every min until no further increase at $A_{\lambda max}$ was detected.

MetaII decay measurements

The MetaII active conformation decay process was followed in real time by fluorescence spectroscopy as previously described [36]. Briefly, 0.5μM Rho in DM buffer, or bicelles buffer, was allowed to stabilize for 10min at 20°C in the fluorimeter, and the sample was subsequently illuminated for 30s with a >495 nm cut-off filter. The increase in Trp fluorescence, due to retinal release from MetaII (which parallels MetaII decay), was monitored, and after reaching a plateau, 50mM of hydroxylamine hydrochloride (pH 7) was added to confirm complete retinal release. The $t_{1/2}$ values for the retinal release curves were determined by fitting the experimental data to single-exponential curves using Sigma Plot version 11.0 (Systat Software, Inc., Chicago, IL, USA).

Chromophore re-entry after photoactivation measured by fluorescence spectroscopy

The retinal re-entry process was monitored in real time by means of fluorescence spectroscopy. 2.5-fold retinal excess over pigment was added into the cuvette, after MetaII was completely decayed, and the changes in fluorescence intensity were

recorded. The volume of the concentrated retinal stock added to the protein sample was 1% of the total sample volume.

RESULTS

UV-vis spectral characterization of purified WT and mutants

WT, G90V and N55K mutants were purified from transfected COS-1 cells, and their UV-visible spectral properties, in either DM buffer (Figure 2) or bicelles buffer (Figure 3), were compared. A summary of the main spectral features of the DM buffer samples, including λ_{max} value of the visible chromophoric band, molar extinction coefficient (ε) and spectral ratio ($A_{280}/A_{\lambda max}$) is shown in Table 1. N55K mutant showed a significantly higher $A_{280}/A_{\lambda max}$ ratio than WT and G90V mutant (Table 1), which implies lower chromophore regeneration. Because 9-*cis*-retinal, and not 11-*cis*-retinal, was used for the regeneration of the recombinant proteins, the WT, G90V and N55K mutants showed visible absorbance bands at 486 nm, 480 nm and 480 nm respectively. Upon illumination, G90V and N55K mutants showed incomplete conversion of the visible band to the 380 nm absorbing species with ~25% remaining absorbance at this wavelength indicating partial trapping of a photointermediate with a protonated SB linkage (Figure 2) [21,30]. WT and G90V showed similar behavior upon illumination in bicelles buffer and in DM buffer. In the case of N55K in bicelles, this mutant showed an altered photobleaching pattern and additional illumination time was required to shift most of the visible band to 380 nm (Figure 3).

DMPC/DHPC stabilization of ROS Rho

DMPC/DHPC bicelles were previously used to increase the thermal stability of purified Rho obtained from ROS membranes [20,26,37]. Here, ROS Rho, solubilized in DM (Rho_{DM}), was purified and used merely as a standard control. In this case, Rho was used to confirm the effectiveness of DMPC/DHPC bicelles in maintaining protein stability. The

decay of the visible band (500 nm) was followed for Rho_{DM} and Rho in bicelles ($Rho_{bicelles}$) at 55ºC (Figure 4) and the $t_{1/2}$ for the process were determined. $T_{1/2}$ for $Rho_{bicelles}$, at 55ºC (41.2±2.5 min) was about 9 fold larger than $t_{1/2}$ for Rho_{DM} (4.7±0.4 min) indicating that DMPC/DHPC bicelles remarkably increase the thermal stability of Rho in comparison to the detergent-solubilized samples, in agreement with previous reports [21,26].

Western blot of WT and G90V, N55K mutants in DM buffer and bicelles buffer

Purified proteins were electrophoretically characterized by means of Western blot analysis (Figure 5). $WT_{bicelles}$ showed higher mobility bands than WT_{DM} and this could be tentatively assigned to oligomeric species of Rho (dimers and higher-order oligomers) although the contribution of protein aggregation cannot be ruled out. G90V showed a prominent characteristic 27KDa band that has been attributed to a truncated form of Rho. This band was detected both in DM and in bicelles. In the case of N55K mutant, $N55K_{bicelles}$ showed a less intense 27 kDa and an apparent increase in the high molecular mass species band when compared to $N55K_{DM}$ pattern.

Thermal Stability of WT and G90V, N55K in DM and in DMPC/DHPC bicelles

WT, G90V and N55K were eluted in either DM buffer or bicelles buffer and their thermal stability was determined at 37 ºC (Figure 6a). Higher temperature, 55ºC, was chosen in previous studies, but the decay process was too fast at this temperature for the $t_{1/2}$ to be determined. At 37ºC, $G90V_{bicelles}$ and $N55K_{bicelles}$ showed enhanced thermal stability when compared to the DM-solubilized samples. Thermal decay process involves protein conformational changes, retinal isomerization and eventually hydrolysis of SB and chromophore release [20,38,39]. We find that $t_{1/2}$ of $G90V_{bicelles}$ and $N55K_{bicelles}$ suffers a 3 and 4 fold increase respectively when compared to the detergent-solubilized samples (Figure 6a and Table 2).

Chromophore regeneration measurements

The effect of DMPC/DHPC bicelles on pigment regeneration after photobleaching was analyzed for the purified proteins. The maximal extent of regeneration and the regeneration rate were the main factors analyzed (Figure 6b). WT regeneration extent was similar for $WT_{bicelles}$ and WT_{DM}. However, $G90V_{bicelles}$ showed 20% more chromophore regeneration than $G90V_{DM}$. Remarkably, N55K exhibited a special behavior because, upon illumination, only 30-40% appeared to be photobleached and the added chromophore did not significantly improve N55K regeneration (Figure 6b and Table 2).

Meta II decay measurements

MetaII stability was studied by fluorescence spectroscopy, which measures retinal release upon sample illumination [36]. Overall, the retinal release process was faster in bicelles than in DM samples. Under both conditions, $t_{1/2}$ values for retinal release followed the order G90V >> WT > N55K, being G90V the slowest (Figure 6c, Figure 7 and Table 2). This behavior may be tentatively associated with the clinical phenotypes caused by these mutations. In all cases, bicelles have decreased the $t_{1/2}$ of the retinal release process for WT (25.4%), G90V (39.8%), and N55K (7.9%) compared with the same process in DM buffer (Figure 6c, Figure 7 and Table 2). Hydroxylamine was added in order to confirm complete retinal release. No changes were detected for the samples in DM buffer (Figure 7A), but in bicelles environment both WT and G90V mutant showed slightly additional increase of Trp fluorescence emission which suggested additional retinal release from the binding pocket (Figure 7B). N55K did not show any increases and kept stable both in DM and bicelles environment (Figure 7A and B). This result is in contrast to that obtained in a previous study in which N55K was in PBS (pH 7.4) containing 0.05% DM [30]. In that case hydroxylamine did cause an

increase in the fluorescence signal which points to a strong effect of buffer in the spectrofluorimetric measurements.

Opsin conformational stability after retinal release

WT and G90V, N55K mutants, in DM buffer or bicelles buffer, were analyzed by fluorescence spectroscopy in order to follow the potential ability of 9-*cis*-retinal to enter the opsin pocket after complete MetaII decay. Thus, 2.5 fold exogenous 9-*cis*-retinal was added, after complete retinal release (plateau in the fluorescence curve), in order to test whether this ligand could enter the binding pocket. WT_{DM} showed only a minor reduction of Trp fluorescence, upon retinal addition, suggesting that the retinal ligand could not significantly enter its binding pocket (Figure 8A). A clear decrease in fluorescence could be detected in the case of $WT_{bicelles}$, indicating that the exogenous chromophore could enter the binding pocket thus quenching Trp fluorescence (Figure 8B). The structurally unstable mutants G90V and N55K showed a clear distinct behavior. Exogenous addition of 9-*cis*-retinal resulted in an important decrease of the fluorescence signal for $G90V_{DM}$ and a further decrease for $G90V_{bicelles}$ (Figure 8). However no change was observed for the N55K either in DM or in bicelles suggesting that this mutation impaired retinal entrance to the binding pocket. Similar results were obtained when the experiments were carried out by using 11-*cis*- retinal (data not shown).

DISCUSSION

Rho mutants (both synthetic and naturally-occurring) have been widely studied to unravel the molecular mechanisms of GPCR activation and signaling, and the molecular mechanisms of RP retinal degenerative disease [16,40,41]. Some of these mutations can cause structural instability and misfolding [42]. The stability of visual photoreceptors, and other GPCRs, has been extensively studied, and several experimental factors, like

temperature, pH, salts, detergents, and lipids have been shown to affect the stability and function of these receptors [8,22,28,43–46]. In spite of this, only limited information is available concerning the molecular causes of the structural instability of mutations in Rho associated with RP. In clear contrast with detergents, lipid bilayers have been shown to increase the stability and facilitate folding, assembly and function of membrane proteins [17,27,28]. Here, we purified the newly reported unstable RP mutants, G90V and N55K, in DMPC/DHPC bicelles. This bicelles system has been proposed to support folding and thermal stability of Rho and opsin [26]. Such a system has been used in solid-state NMR studies of membrane-associated molecules and its use extended to non-NMR-based biophysical studies of transmembrane proteins [27,47–49].

The structural arrangement of Rho in DM and in bicelles show important differences. DM would form micelles to embed Rho, whereas DMPC and DHPC shaped bicelles that could better mimic the membrane environment (Figure 1). The UV-visible characterization of WT, N55K and G90V in DM detergent was done with 9-*cis*-retinal regenerated samples. The 9-*cis* isomer was used because it has been previously shown that this isomer can improve chromophore regeneration of Rho mutants [21]. The visible bands of the WT and the mutants where blue-shifted, with regard to the 11-*cis*-retinal containing samples, due to the specific interaction of 9-*cis*-retinal with the amino acids in the binding pocket. N55K mutant showed higher $A_{280}/A_{\lambda max}$ than WT in DM buffer, which could imply lower chromophore stability during the purification process, as previously described [30]. The two mutations studied, G90V and N55K, showed abnormal photobleaching behavior, in DM buffer, with incomplete conversion of the visible band upon illumination (Figure 2). In bicelles buffer, G90V showed WT-like behaviour but N55K showed an altered photobleaching pattern (Figure 3) indicating that bicelles stabilized either its dark state or a photointermediate conformation. Electrophoretic

analysis of the purified mutant proteins revealed differences in the intensities of bands that would correspond to dimeric (or higher-order oliogomeric) conformations that appeared to be favoured in bicelles.. Interestingly, G90V and N55K mutants showed the presence of lower bands in the 25-30 Kda range, particularly a 27 kDa band that has been attributed to a truncated form of opsin [50,51]. This behavior suggests that the mutants may have increased susceptibility to protein truncation which may be associated with a decreased conformational stability, and may be linked to the molecular phenotype underlying the pathological nature of the mutations.

Thermal stability for the mutants at 37ºC has been clearly improved in the bicelles system. In particular, $N55K_{bicelles}$ showed a 4-fold increase in thermal stability compared with $N55K_{DM}$, at this temperature, meaning that bicelles provide conformational stability and protect the SB linkage from hydrolysis [39]. Chromophore regeneration represents also an important index that reflects structural stability of Rho mutants. $G90V_{bicelles}$ showed a 20% chromophore regeneration increase compared to $G90V_{DM.}$ From the fluorescence experiments, this mutant also showed increased retinal entry into the binding pocket long time after illumination, in the bicelles sample, suggesting that lipids play a role in the regeneration process by helping stabilize its optimal ligand-binding conformation. In contrast, N55K did not show any improvement in chromophore regeneration which is consistent with the mutation impairing retinal release due to specific interactions at the transmembrane domain of the receptor. This trend would be maintained in the case of this mutant in the bicelles environment.

In the MetaII decay experiment, after the sample was illuminated and the active MetaII conformation decayed, subsequent hydroxylamine addition resulted in additional fluorescence increase for $WT_{bicelles}$ and $G90D_{bicelles}$. This suggests that bicelles can increase the residence time of all-*trans*-retinal in the binding pocket thus extending the

available time for G-protein activation [6]. On the contrary, N55K did not show any difference, after hydroxylamine addition, either in DM detergent or in bicelles buffer. We have previously reported that in PBS with 0.05% DM could increase the fluorescence signal [30]. Thus, the buffer conditions clearly influence the fluorescence assay.

The fluorescence decrease upon retinal addition, after complete MetaII decay (Figure 8), would indicate that retinal can enter the retinal binding pocket although this does not demonstrate covalent binding to the opsin moiety. This suggests that bicelles help maintaining a stable opsin structure long time after complete retinal release process thus favoring retinal binding to the protein. Interestingly, N55K did not show any decrease, either in DM or in bicelles, and this is a differential effect only seen for this mutant that may be associated with the sector RP phenotype restricted mostly to the inferior quadrants of the retina [19]. This unique N55K behavior may provide new clues that would guide us into deciphering the molecular mechanism of sector RP. We have previously associated this mechanism with different response to light by this mutant [30].

Both the two mutations studied, N55K and G90D, correspond to amino acids which are facing to the protein interior and are mainly involved in helix-helix interactions. Thus, residues at 55 and 90 are not facing the lipid or involved in monomer-monomer interactions (Figure 9). Furthermore, the residues do not appear to significantly alter their orientation (or interactions) in the activated state of the receptor [12].

In the case of N55K, this mutation is located at transmembrane helix 1 in a region closer to the cytoplasmic side of the protein where the G-protein activation process takes place. Three highly conserved residues, throughout the GPCRs superfamily, towards the cytoplasmic side of the receptor, N55 (98%), D83 (92%) and N302 (77%), define a region with intimate contact between TMs 1, 2 and 7, which involves also various highly conserved water molecules. In the N55K substitution, the Lys side-chain would interfere with these contacts and could form

a salt bridge with D83 (Figure 9). The G90V mutation affects an amino acid, at transmembrane helix 2, which is located towards the intradiscal domain of the protein that plays a structural role in the folding of the receptor and in the retinal binding process. The reported G90V mutant behavior suggests an important role for a functional water molecule present in the vicinity of E113 and the SB in the dark-state crystal structure of Rho [21]. This water molecule binds to both the carbonyl backbone and one of the carboxyl oxygens of E113. The lack of a side-chain at G90 gives an empty volume that is filled with such a water molecule, whereas the hydrophobic chain in G90V would either not allow the water molecule to be accommodated or result in a smaller affinity. The lack of the water molecule would alter the metarhodopsin I to MetaII transition energy landscape and would also decrease dark-state stability, in agreement with the present results [21].

The influence of membrane morphology and composition on receptor structure and function is undoubtedly a key factor to take into account when analyzing the effect of mutations particularly of those associated with disease. We have reported a significant effect of DMPC/DHPC bicelles in the stabilization of Rho mutants associated with RP retinal disease. In the case of G90V, a significant increase in the chromophore thermal stability and regeneration was observed which is likely due to the stabilizing effect of the lipid bicelles on the opsin conformation of the mutant. The other studied mutant, N55K associated to the peculiar sector RP phenotype [30], shows also improved thermal stability but no improvement in its retinal regeneration ability. This would be due to the specificity imposed by the Lys introduced in the transmembrane domain of the photoreceptor protein [30] that would entrap the retinal molecule impairing efficient retinal regeneration after photobleaching. Overall, our results underscore the importance of the topological arrangement of lipids in stabilizing critical interhelical interactions and promoting favorable helical packing forces that would be absent in detergent-solubilized samples. Further in-depth studies on the structural and energetic features of

the lipid-protein interactions are needed for deciphering the structural basis of the differential stability seen for Rho mutations. This knowledge is important in order to provide functionally-relevant structural information that can be useful in the development of targeted therapies towards retinal degenerative diseases.

ACKNOWLEDGEMENTS

The authors want to thank Sundaramoorthy Srinivasan, Miguel A. Fernández Sampedro and Margarita Morillo for helpful discussions.

REFERENCES

(1) Fredriksson, R., Lagerstrom, M. C., Lundin, L.-G., and Schioth, H. B. (2003) The G-protein-coupled receptors in the human genome form five main families. Phylogenetic analysis, paralogon groups, and fingerprints. *Molecular pharmacology 63*, 1256–1272.

(2) Tesmer, J. J. G. (2010) The quest to understand heterotrimeric G protein signaling. *Nat Struct Mol Biol 17*, 650–652.

(3) Hiller, C., Kuhhorn, J., and Gmeiner, P. (2013) Class A G-protein-coupled receptor (GPCR) dimers and bivalent ligands. *Journal of medicinal chemistry 56*, 6542–6559.

(4) Rosenbaum, D. M., Rasmussen, S. G. F., and Kobilka, B. K. (2009) The structure and function of G-protein-coupled receptors. *Nature 459*, 356–363.

(5) Venkatakrishnan, A. J., Deupi, X., Lebon, G., Tate, C. G., Schertler, G. F., and Babu, M. M. (2013) Molecular signatures of G-protein-coupled receptors. *Nature 494*, 185–194.

(6) Wang, Y., Botelho, A. V., Martinez, G. V, and Brown, M. F. (2002) Electrostatic properties of membrane lipids coupled to metarhodopsin II formation in visual transduction. *Journal of the American Chemical Society 124*, 7690–7701.

(7) Gibson, N. J., and Brown, M. F. (1991) Membrane lipid influences on the energetics of the metarhodopsin I and metarhodopsin II conformational states of rhodopsin probed by flash photolysis. *Photochemistry and photobiology 54*, 985–992.

(8) Huber, T., Rajamoorthi, K., Kurze, V. F., Beyer, K., and Brown, M. F. (2002) Structure of docosahexaenoic acid-containing phospholipid bilayers as studied by (2)H NMR and molecular dynamics simulations. *Journal of the American Chemical Society 124*, 298–309.

(9) Boesze-Battaglia, K., and Schimmel, R. (1997) Cell membrane lipid composition and distribution: implications for cell function and lessons learned from photoreceptors and platelets. *The Journal of experimental biology 200*, 2927–2936.

(10) Hernandez-Rodriguez, E. W., Sanchez-Garcia, E., Crespo-Otero, R., Montero-Alejo, A. L., Montero, L. A., and Thiel, W. (2012) Understanding rhodopsin mutations linked to the retinitis pigmentosa disease: a QM/MM and DFT/MRCI study. *The journal of physical chemistry. B 116*, 1060–1076.

(11) Lamb, T. D., and Pugh, E. N. J. (2006) Phototransduction, dark adaptation, and rhodopsin regeneration the proctor lecture. *Investigative ophthalmology & visual science 47*, 5137–5152.

(12) Hofmann, K. P., Scheerer, P., Hildebrand, P. W., Choe, H.-W., Park, J. H., Heck, M., and Ernst, O. P. (2009) A G protein-coupled receptor at work: the rhodopsin model. *Trends in biochemical sciences 34*, 540–552.

(13) Yau, K.-W., and Hardie, R. C. (2009) Phototransduction motifs and variations. *Cell 139*, 246–264.

(14) Daiger, S. P., Sullivan, L. S., and Bowne, S. J. (2013) Genes and mutations causing retinitis pigmentosa. *Clinical genetics 84*, 132–141.

(15) Rayapudi, S., Schwartz, S. G., Wang, X., and Chavis, P. (2013) Vitamin A and fish oils for retinitis pigmentosa. *The Cochrane database of systematic reviews 12*, CD008428.

(16) Krebs, M. P., Holden, D. C., Joshi, P., Clark, C. L. 3rd, Lee, A. H., and Kaushal, S. (2010) Molecular mechanisms of rhodopsin retinitis pigmentosa and the efficacy of pharmacological rescue. *Journal of molecular biology 395*, 1063–1078.

(17) Saliba, R. S., Munro, P. M. G., Luthert, P. J., and Cheetham, M. E. (2002) The cellular fate of mutant rhodopsin: quality control, degradation and aggresome formation. *Journal of cell science 115*, 2907–2918.

(18) Ulloa-Aguirre, A., Zarinan, T., Dias, J. A., and Conn, P. M. (2014) Mutations in G protein-coupled receptors that impact receptor trafficking and reproductive function. *Molecular and cellular endocrinology 382*, 411–423.

(19) Van Woerkom, C., and Ferrucci, S. (2005) Sector retinitis pigmentosa. *Optometry (St. Louis, Mo.) 76*, 309–317.

(20) Ramon, E., Marron, J., del Valle, L., Bosch, L., Andres, A., Manyosa, J., and Garriga, P. (2003) Effect of dodecyl maltoside detergent on rhodopsin stability and function. *Vision research 43*, 3055–3061.

(21) Toledo, D., Ramon, E., Aguila, M., Cordomi, A., Perez, J. J., Mendes, H. F., Cheetham, M. E., and Garriga, P. (2011) Molecular mechanisms of disease for mutations at Gly-90 in rhodopsin. *The Journal of biological chemistry 286*, 39993–40001.

(22) Sanchez-Martin, M. J., Ramon, E., Torrent-Burgues, J., and Garriga, P. (2013) Improved conformational stability of the visual G protein-coupled receptor rhodopsin by specific interaction with docosahexaenoic acid phospholipid. *Chembiochem□: a European journal of chemical biology 14*, 639–644.

(23) Tsukamoto, H., Szundi, I., Lewis, J. W., Farrens, D. L., and Kliger, D. S. (2011) Rhodopsin in nanodiscs has native membrane-like photointermediates. *Biochemistry 50*, 5086–5091.

(24) Reeves, P. J., Hwa, J., and Khorana, H. G. (1999) Structure and function in rhodopsin: kinetic studies of retinal binding to purified opsin mutants in defined phospholipid-detergent mixtures serve as probes of the retinal binding pocket. *Proceedings of the National Academy of Sciences of the United States of America 96*, 1927–1931.

(25) Serebryany, E., Zhu, G. A., and Yan, E. C. Y. (2012) Artificial membrane-like environments for in vitro studies of purified G-protein coupled receptors. *Biochimica et biophysica acta 1818*, 225–233.

(26) McKibbin, C., Farmer, N. A., Jeans, C., Reeves, P. J., Khorana, H. G., Wallace, B. A., Edwards, P. C., Villa, C., and Booth, P. J. (2007) Opsin stability and folding: modulation by phospholipid bicelles. *Journal of molecular biology 374*, 1319–1332.

(27) Sanders, C. R., and Prosser, R. S. (1998) Bicelles: a model membrane system for all seasons? *Structure (London, England□: 1993) 6*, 1227–1234.

(28) Kaya, A. I., Thaker, T. M., Preininger, A. M., Iverson, T. M., and Hamm, H. E. (2011) Coupling efficiency of rhodopsin and transducin in bicelles. *Biochemistry 50*, 3193–3203.

(29) Neidhardt, J., Barthelmes, D., Farahmand, F., Fleischhauer, J. C., and Berger, W. (2006) Different amino acid substitutions at the same position in rhodopsin lead to distinct phenotypes. *Investigative ophthalmology & visual science 47*, 1630–1635.

(30) Ramon, E., Cordomi, A., Aguila, M., Srinivasan, S., Dong, X., Moore, A. T., Webster, A. R., Cheetham, M. E., and Garriga, P. (2014) Differential light-induced responses in sectorial inherited retinal degeneration. *The Journal of biological chemistry 289*, 35918–35928.

(31) Sekharan, S., and Morokuma, K. (2011) Why 11-cis-retinal? Why not 7-cis-, 9-cis-, or 13-cis-retinal in the eye? *Journal of the American Chemical Society 133*, 19052–19055.

(32) Srinivasan, S., Ramon, E., Cordomi, A., and Garriga, P. (2014) Binding specificity of retinal analogs to photoactivated visual pigments suggest mechanism for fine-tuning GPCR-ligand interactions. *Chemistry & biology 21*, 369–378.

(33) Oprian, D. D., Molday, R. S., Kaufman, R. J., and Khorana, H. G. (1987) Expression of a synthetic bovine rhodopsin gene in monkey kidney cells. *Proceedings of the National Academy of Sciences of the United States of America 84*, 8874–8878.

(34) Longo, P. A., Kavran, J. M., Kim, M.-S., and Leahy, D. J. (2013) Transient mammalian cell transfection with polyethylenimine (PEI). *Methods in enzymology 529*, 227–240.

(35) Hacker, D. L., Kiseljak, D., Rajendra, Y., Thurnheer, S., Baldi, L., and Wurm, F. M. (2013) Polyethyleneimine-based transient gene expression processes for suspension-adapted HEK-293E and CHO-DG44 cells. *Protein expression and purification 92*, 67–76.

(36) Farrens, D. L., and Khorana, H. G. (1995) Structure and function in rhodopsin. Measurement of the rate of metarhodopsin II decay by fluorescence spectroscopy. *The Journal of biological chemistry 270*, 5073–5076.

(37) Jastrzebska, B., Debinski, A., Filipek, S., and Palczewski, K. (2011) Role of membrane integrity on G protein-coupled receptors: Rhodopsin stability and function. *Progress in lipid research 50*, 267–277.

(38) Fotiadis, D., Liang, Y., Filipek, S., Saperstein, D. A., Engel, A., and Palczewski, K. (2003) Atomic-force microscopy: Rhodopsin dimers in native disc membranes. *Nature 421*, 127–128.

(39) Liu, J., Liu, M. Y., Nguyen, J. B., Bhagat, A., Mooney, V., and Yan, E. C. Y. (2009) Thermal Decay of Rhodopsin: Role of Hydrogen Bonds in Thermal Isomerization of 11- cis Retinal in the Binding Site and Hydrolysis of Protonated Schiff Base *19*, 8750–8751.

(40) Golovleva, I., Bhattacharya, S., Wu, Z., Shaw, N., Yang, Y., Andrabi, K., West, K. A., Burstedt, M. S. I., Forsman, K., Holmgren, G., Sandgren, O., Noy, N., Qin, J., and Crabb, J. W. (2003) Disease-causing mutations in the cellular retinaldehyde binding protein tighten and abolish ligand interactions. *The Journal of biological chemistry 278*, 12397–12402.

(41) Petrs-Silva, H., and Linden, R. (2014) Advances in gene therapy technologies to treat retinitis pigmentosa. *Clinical ophthalmology (Auckland, N.Z.) 8*, 127–136.

(42) Tzekov, R., Stein, L., and Kaushal, S. (2011) Protein misfolding and retinal degeneration. *Cold Spring Harbor perspectives in biology 3*, a007492.

(43) Rozin, R., Wand, A., Jung, K.-H., Ruhman, S., and Sheves, M. (2014) pH dependence of Anabaena sensory rhodopsin: retinal isomer composition, rate of dark adaptation, and photochemistry. *The journal of physical chemistry. B 118*, 8995–9006.

(44) Parkes, J. H., Gibson, S. K., and Liebman, P. A. (1999) Temperature and pH dependence of the metarhodopsin I-metarhodopsin II equilibrium and the binding of metarhodopsin II to G protein in rod disk membranes. *Biochemistry 38*, 6862–6878.

(45) Alves, I. D., Salgado, G. F. J., Salamon, Z., Brown, M. F., Tollin, G., and Hruby, V. J. (2005) Phosphatidylethanolamine enhances rhodopsin photoactivation and transducin binding in a solid supported lipid bilayer as determined using plasmon-waveguide resonance spectroscopy. *Biophysical journal 88*, 198–210.

(46) Sato, K., Morizumi, T., Yamashita, T., and Shichida, Y. (2010) Direct observation of the pH-dependent equilibrium between metarhodopsins I and II and the pH-independent interaction of metarhodopsin II with transducin C-terminal peptide. *Biochemistry 49*, 736–741.

(47) Sanders, C. R., and Oxenoid, K. (2000) Customizing model membranes and samples for NMR spectroscopic studies of complex membrane proteins 1 *1508*, 129–145.

(48) Fernández, C., Hilty, C., Wider, G., and Wüthrich, K. (2002) Lipid-protein interactions in DHPC micelles containing the integral membrane protein OmpX investigated by NMR spectroscopy. *Proceedings of the National Academy of Sciences of the United States of America 99*, 13533–13537.

(49) Marcotte, I., and Auger, M. (2005) Bicelles as model membranes for solid-and solution-state NMR studies of membrane peptides and proteins. *Concepts in Magnetic Resonance Part A: Bridging Education and Research 24*, 17–35.

(50) Janz, J. M., Fay, J. F., and Farrens, D. L. (2003) Stability of dark state rhodopsin is mediated by a conserved ion pair in intradiscal loop E-2. *Journal of Biological Chemistry 278*, 16982–16991.

(51) Sung, C. H., Schneider, B. G., Agarwal, N., Papermaster, D. S., and Nathans, J. (1991) Functional heterogeneity of mutant rhodopsins responsible for autosomal dominant retinitis pigmentosa. *Proceedings of the National Academy of Sciences of the United States of America 88*, 8840–8844.

Table 1. ***Spectroscopic properties of WT and RP mutants purified in DM buffer***. [a]Mean values of the visible λ_{max} of WT and RP mutants G90V, N55K in DM buffer. [b]Each ε value was calculated with the equation: $\varepsilon=(A/A_{Rho})(A_{440Rho}/A_{440})\ \varepsilon_{Rho}$. Where A is the absorbance at the λ_{max} value, A_{440} is the absorbance at 440 nm after acid denaturation, and the ε_{Rho} is the molar extinction of Rho (42.7×10^3 $M^{-1}cm^{-1}$) [21]. [c]The A_{280}/A_{max} ratio reflects the extent of chromophore regeneration. All values were determined from 3 independent experiments

Opsin	[a]λ_{max} (nm)	[b]ε x 10^3 ($M^{-1}cm^{-1}$)	[c]$A_{280}/A\ \lambda_{max}$
WT	486±3	43.2±0.1	2.4±0.1
G90V	480±3	34.1±0.5	3.0±0.3
N55K	480±2	35.5±0.3	5.1±1.6

Table 2. ***Molecular properties of WT and RP mutants from thermal stability, chromophore regeneration and MetaII decay experiments in DM and bicelles.*** [a]$t_{1/2}$ of WT and G90V, N55K mutants in thermal bleaching experiments. Thermal decay experiments were run at 37°C. At the end of the thermal decay, 50 mM hydroxylamine (pH 7.0) was added to confirm complete decay. Curves were fit to an exponential decay function. [b]*Regeneration percentage of WT and G90V, N55K mutants*. Retinal was added before illumination and spectra were recorded every min after illuminating the samples for 30s. These experiments were run at 20ºC. [c]*Retinal release $t_{1/2}$ of WT and G90V, N55K mutants*. Samples were stabilized for 10min in the dark and subsequently illuminated for 30s (λ> 495nm). Fluorescence increase was measured until the signal reached a plateau. 50mM hydroxylamine pH 7.0 was added to confirm complete retinal release. The $t_{1/2}$ of the retinal release was determined from the exponential curves.

	Buffer	WT	G90V	N55K
[a]Thermal bleaching	DM	> 180 min	22.5±3.1 min	30.1±1.7 min
	bicelles	> 180 min	64.1±3.7 min	123.5±2.6 min
[b]Regeneration	DM	91.8 ± 3.2%	70.8 ± 3.3%	11.7 ± 1.9%
	bicelles	88.9 ± 3.2%	96.2 ± 2.3%	16.9 ± 2.1%
[c]MetaII decay	DM	19.3±0.5 min	34.9±1.0 min	10.1±1.5min
	bicelles	14.4±1.7 min	21.0±2.6 min	9.3±2.1 min

Figures legends

Figure 1. Schematic models for Rho in DM micelles and in DMPH/DHPC bicelles. (A) Schematic model for DM micelles with Rho. The hydrophobic tail of DM can wrap the hydrophobic transmembrane domain of the protein which is embedded in the core of the micelle. (B) Schematic model of DMPC-DHPC bicelles with embedded Rho. DMPC and DHPC form a bilayer structure.

Figure 2. UV-vis characterization of WT, N55K and G90V in DM buffer. WT, G90V and N55K mutants were immunopurified in DM buffer with 0.05% DM. The spectra were measured at 20ºC. Illumination was carried out for 30s with a 150-watt power source equipped with an optic fiber guide using a >495nm cut-off filter to avoid photobleaching of the free retinal. (—) Dark state. (····) photobleached state; inset, difference spectrum (dark-light).

Figure 3. UV-vis difference spectra of the WT and N55K, G90V in bicelles before and after illumination. WT, G90V and N55K mutants were purified in bicelles buffer. The spectra were measured at 20ºC. (—) Dark state. (····), photobleached state. Illumination was carried out for 30s with a 150-watt power source equipped with an optic fiber guide using a >495nm cut-off filter to avoid photobleaching of the free retinal. Notably, $N55K_{bicelles}$ showed only 20% photobleaching (a), illumination for a further 30s caused further A_{max} decay (b).

Figure 4. DMPC/DHPC stabilization of Rho from ROS. A, Thermal Stability of Rho from ROS in either DM or bicelles at 55°C. Purified Rho was dissolved in either DM

buffer -- Rho_{DM} (•) or in bicelles buffer -- $Rho_{bicelles}$ (o). Spectra were recorded at 55°C and normalized absorbance values at the Amax were plotted over time. Spectra were recorded every min. At the end of the thermal decay, 50 mM hydroxylamine (pH 7.0) was added to confirm complete decay. Curves were fit to an exponential decay function.

Figure 5. Western blot of WT and G90V, N55K in either DM detergent or bicelles conditions. WT, G90V and N55K mutants were purified from COS-1 cells either in DM buffer or bicelles buffer respectively. The same amount of protein was loaded onto an SDS-PAGE gel, subject to electrophoresis and subsequently transferred to a nitrocellulose membrane for detection. $WT_{bicelles}$ and $N55K_{bicelles}$ showed more higher-molecular species than WT_{DM} and $N55K_{DM}$. The two mutants showed clear bands below the main opsin band that could correspond to truncated Rho or to non-glyscosylated species.

Figure 6. Conformational properties of WT and RP mutants from thermal stability, chromophore regeneration and MetaII decay experiments. WT and G90V, N55K were purified in DM buffer (black bar) and bicelles buffer (gray bar). a) $t_{1/2}$ of WT, G90V and N55K mutants from thermal bleaching experiments at 37°C; b) chromophore regeneration percentage of WT and G90V, N55K mutants; c) $t_{1/2}$ of WT and G90V, N55K mutants in MetaII decay experiments. The numerical values for the measured times are displayed in Table 2. The mean and error bars of three independent measurements are represented.

Figure 7. MetaII decay for WT and G90V, N55K mutants. WT and G90V, N55K were purified in either DM buffer (panel A) or in bicelles buffer (panel B). The samples were

illuminated for 30s (> 495nm) after the dark-state fluorescence intensity was stabilized. After MetaII decay and once the fluorescence intensity reached plateau, 50mM hydroxylamine pH 7.0 was added to confirm complete retinal release.

Figure 8. Retinal entry in photoactivated opsin . After fluorescence intensity reached a plateau, from MetaII decay experiment, for WT, N55K and G90V pigments purified either in DM buffer (panel A) or bicelles buffer (panel B), retinal was added (2.5 fold of exogenous retinal to the concentration of pigment) and mixed well to detect retinal entry into the binding pocket. $WT_{bicelles}$ and $G90V_{bicelles}$ showed more fluorescence decrease than the DM samples, whereas $N55K_{bicelles}$ did not show any change upon retinal addition.

Figure 9. ***Structural model of Rho showing the sites of mutations***. Lys at position 55 (red) and Val at position 90 (yellow) are shown together with other relevant molecules, like retinal (green), Asp83 (blue) and water (magenta). Although the two mutations are located at the transmembrane domain of the protein, Lys55 is closer to the cytoplasmic domain where the G-protein activating function of the receptor takes place, whereas Val90 is closer to the retinal binding site and the intradiscal domain, a region of the protein that governs its folding and stability. Rho dark-state crystal structure (PDB id 3C9L) was used and the image was created using PyMol (Schrodinger, LLC. The PyMOL Molecular Graphics System, Version 1.5).

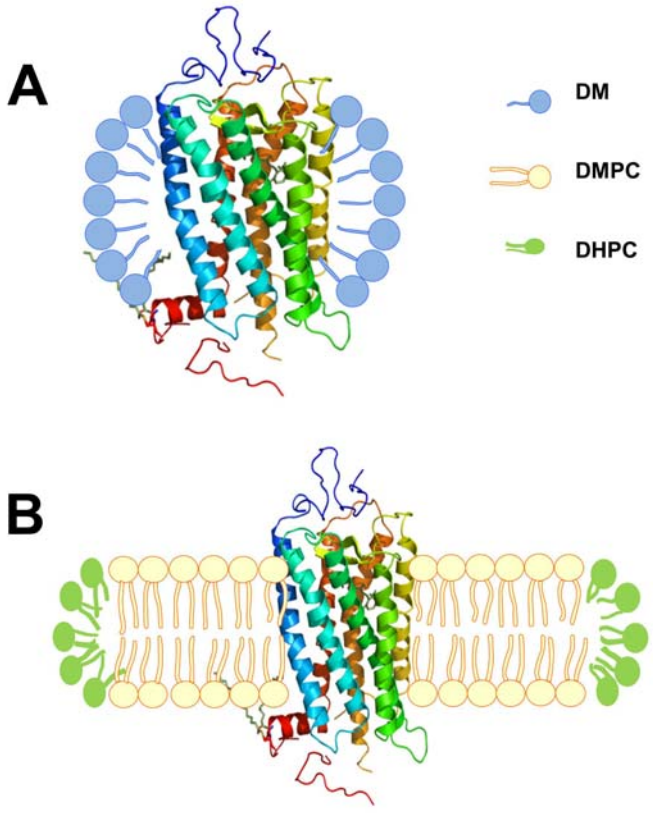

Figure 1

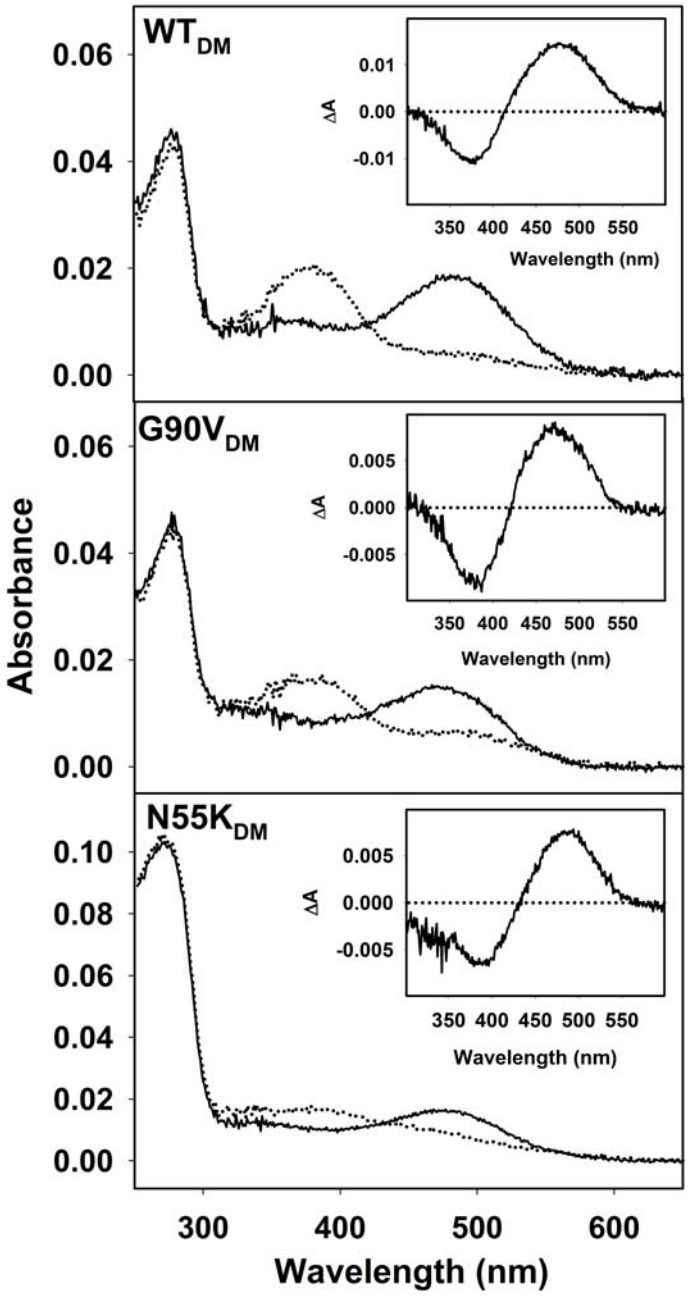
WT DM
G90V DM
N55K DM
Absorbance
Wavelength (nm)
ΔA
0.06
0.04
0.02
0.00
0.10
0.08
0.01
-0.01
0.005
0.000
-0.005
300
400
500
600
350 400 450 500 550

Figure 2

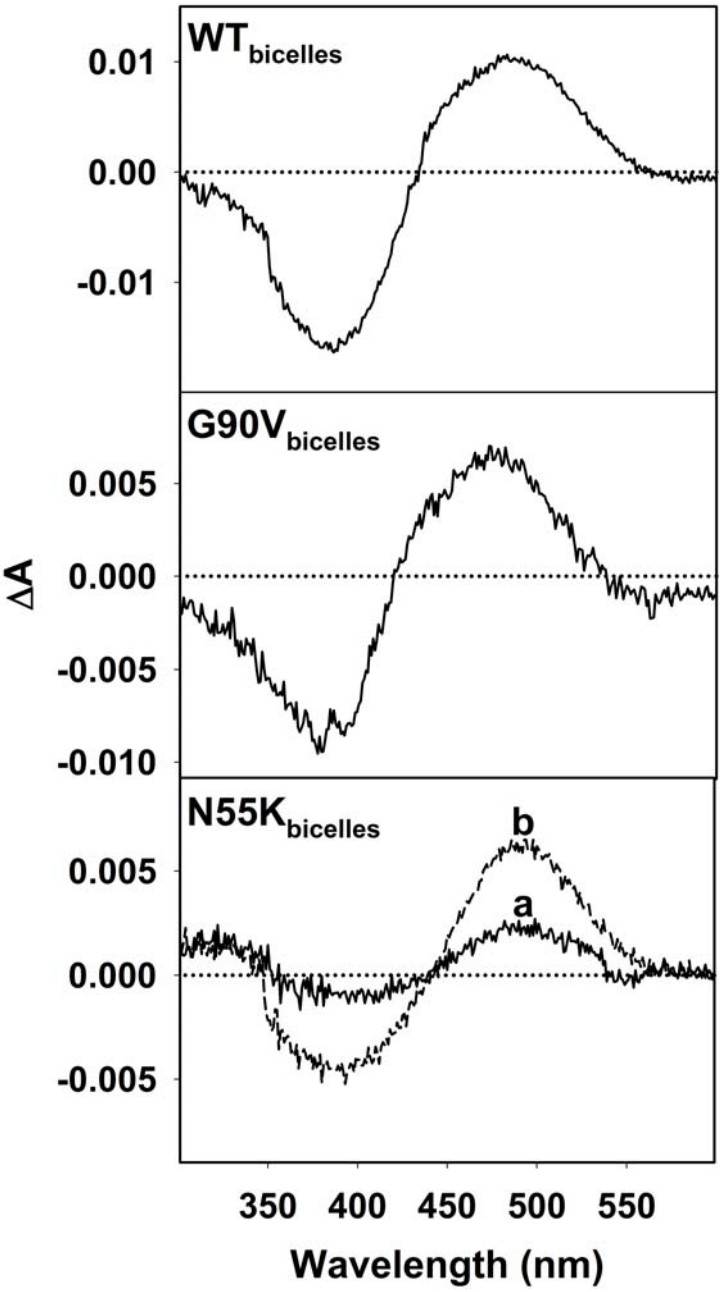
WT bicelles
0.01
0.00
-0.01
G90V bicelles
0.005
0.000
-0.005
-0.010
N55K bicelles
b
a
0.005
0.000
-0.005
ΔA
350
400
450
500
550
Wavelength (nm)

Figure 3

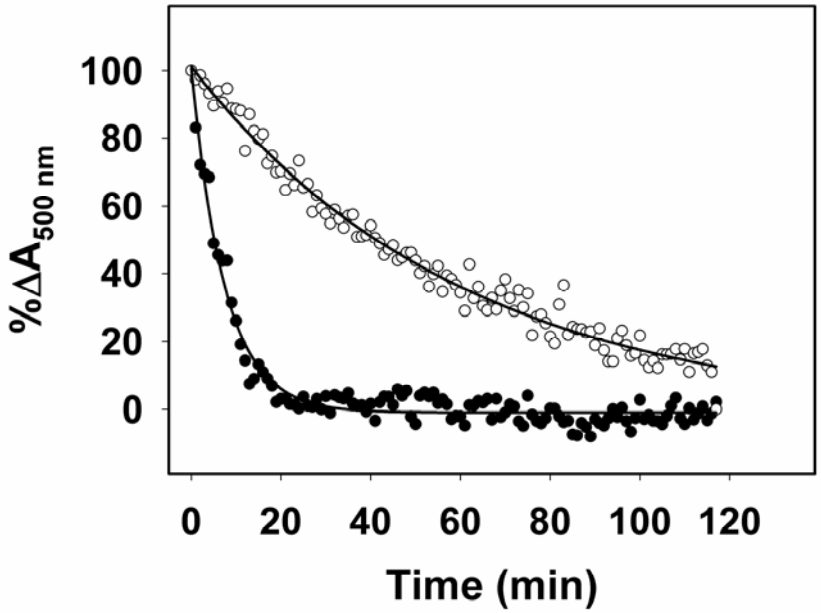

Figure 4

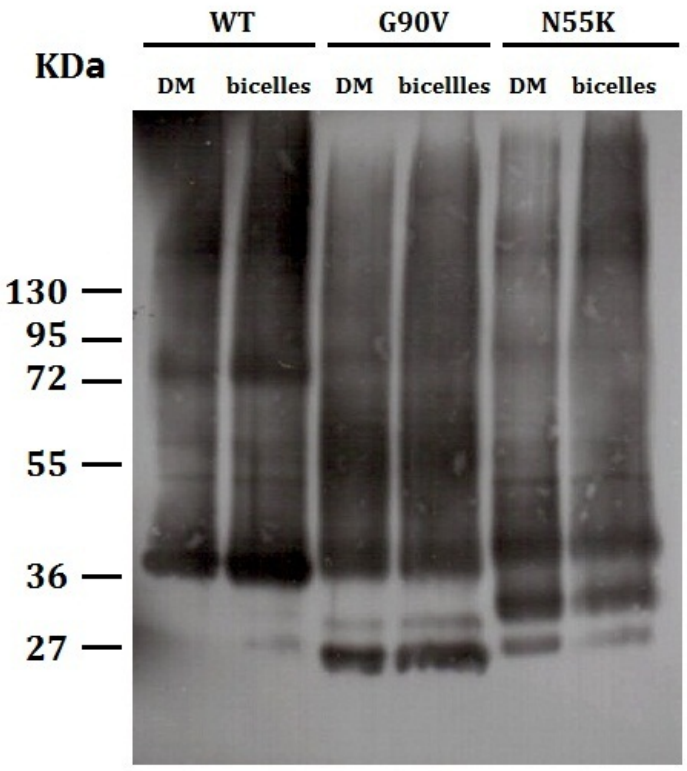
WT
G90V
N55K
KDa
DM
bicelles
DM
bicellles
DM
bicelles
130
95
72
55
36
27

Figure 5

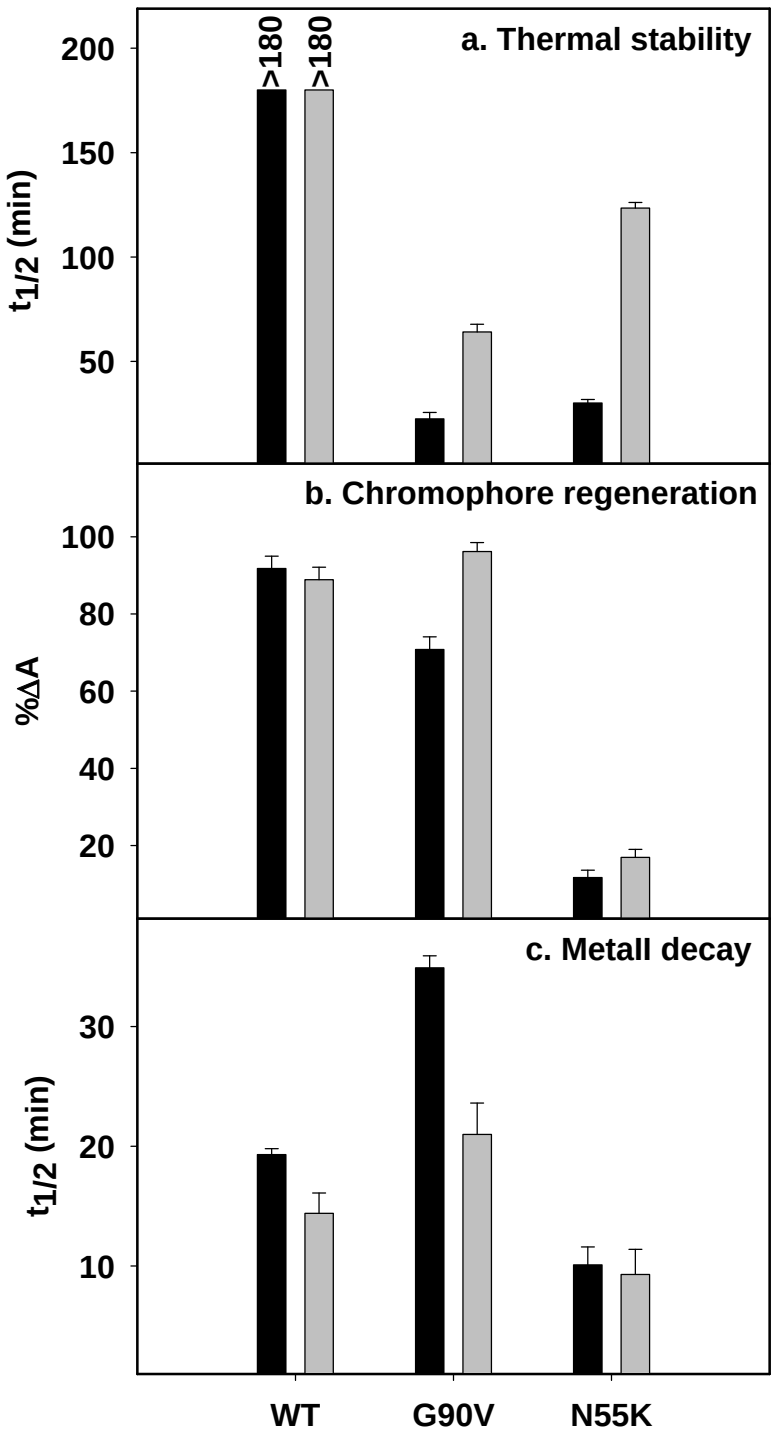
a. Thermal stability
>180
>180
200
150
100
50
t1/2 (min)
b. Chromophore regeneration
100
80
60
40
20
%ΔA
c. MetaII decay
30
20
10
t1/2 (min)
WT
G90V
N55K

Figure 6

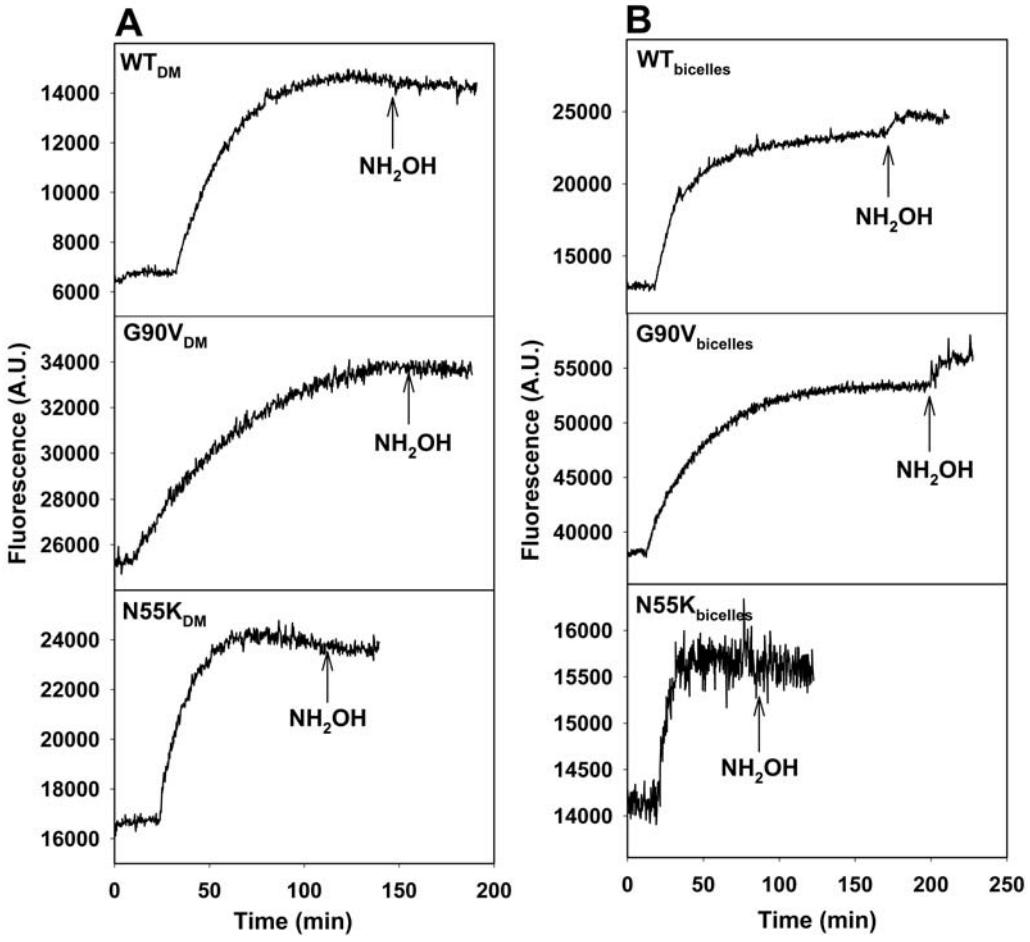
A
WT$_{DM}$
G90V$_{DM}$
N55K$_{DM}$
NH$_2$OH
Fluorescence (A.U.)
Time (min)
B
WT$_{bicelles}$
G90V$_{bicelles}$
N55K$_{bicelles}$
NH$_2$OH
Fluorescence (A.U.)
Time (min)

Figure 7

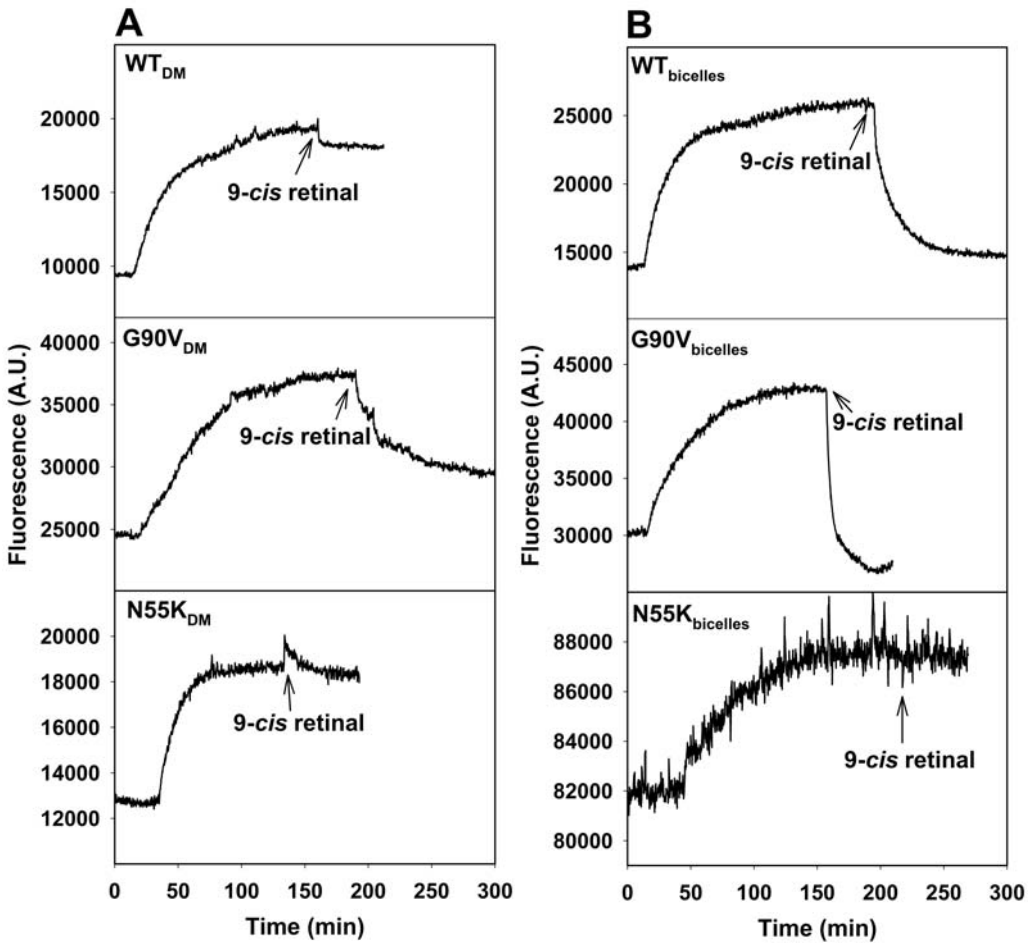
A
WT DM
20000
15000
10000
9-cis retinal
G90V DM
40000
35000
30000
25000
9-cis retinal
N55K DM
20000
18000
16000
14000
12000
9-cis retinal
Fluorescence (A.U.)
0
50
100
150
200
250
300
Time (min)
B
WT bicelles
25000
20000
15000
9-cis retinal
G90V bicelles
45000
40000
35000
30000
9-cis retinal
N55K bicelles
88000
86000
84000
82000
80000
9-cis retinal
Fluorescence (A.U.)
0
50
100
150
200
250
300
Time (min)

Figure 8

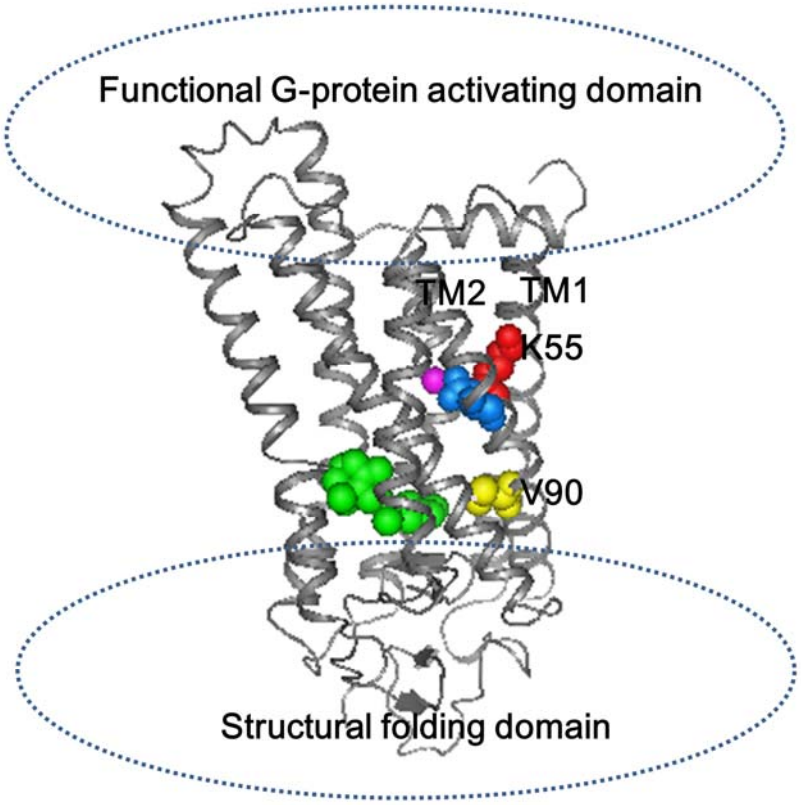
Functional G-protein activating domain
TM2
TM1
K55
V90
Structural folding domain

Figure 9